

Chaotic dynamics of vortices in the plastic phase

E. Olive, J.C. Soret

LEMA, UMR 6157, Université François Rabelais - CNRS - CEA, Parc de Grandmont 37200 Tours, France

(Dated: 20th October 2019)

We present numerical simulation results of driven vortex lattices in presence of random disorder at zero temperature. We show that the plastic dynamics is readily understood in the framework of chaos theory. Intermittency "routes to chaos" have been clearly identified, and positive Lyapunov exponents and broad-band noise, both characteristic of chaos, are found to coincide with the differential resistance peak.

PACS numbers: **74.25.Qt, 74.40.+k, 05.45.Pq**

When flowing over a random medium, vortices in type II superconductors display a great variety of dynamical regimes, from the depinning threshold up to the high driving phase. Most of the $V - I$ experiments [1, 2] and numerical simulations [3, 4, 5, 6, 7] reveal an intricate interplay between the 'peak effect' (PE), *i.e.* the increase of the depinning threshold current below the upper critical field H_{c2} , the peak of the differential resistance dV/dI , voltage noise and plastic flow of vortices. Below the PE an ordered phase is expected and the unusual excess noise measurements are understood within an edge contamination process where a metastable disordered vortex phase generated at the edges is annealed into an ordered phase in the bulk [8]. On the contrary, in the PE region a disordered phase is expected and plasticity effects such as tearing are expected at the depinning threshold. These features have recently been studied in the mean field approach [9]. However many open questions about the complex plastic flow remain, and in particular its dynamical properties.

In this Letter, we propose to examine the plastic phase through the chaos theory of deterministic dissipative dynamical systems. Charge density waves and Josephson junctions arrays have already been analysed through chaos theory [10], but such study is completely new for vortex lattices. We performed numerical simulations that clearly demonstrate the chaotic behavior of vortices in the plastic phase. While increasing the driving force, instabilities are developed by the non-linearities of the system and periodic regimes are destabilized giving rise to chaotic regimes. Such destabilizations have been clearly identified in our system to be the intermittency "route to chaos". The voltage noise and the Lyapunov exponents are used to characterize the chaotic phase which is shown to coincide with the peak of dV/dI . Therefore within the framework of chaotic dynamical systems, our results open new perspectives in the understanding of vortex dynamics that are discussed in the conclusion.

We consider N_v Abrikosov vortices driven over a random pinning background in the (x, y) plane. At $T = 0$

the overdamped equation of motion of a vortex i in position \mathbf{r}_i reads

$$\eta \frac{d\mathbf{r}_i}{dt} = - \sum_{j \neq i} \nabla_i U^{vv}(r_{ij}) - \sum_p \nabla_i U^{vp}(r_{ip}) + \mathbf{F}^L \quad (1)$$

where r_{ij} is the distance between vortices i and j , r_{ip} is the distance between the vortex i and the pinning site located at \mathbf{r}_p , and ∇_i is the 2D gradient operator acting in the (x, y) plane. The viscosity coefficient is η , $\mathbf{F}^L = F^L \hat{\mathbf{x}}$ is the Lorentz driving force due to an applied current. The vortex-vortex pairwise repulsive interaction is given by a modified Bessel function $U^{vv}(r_{ij}) = 2\epsilon_0 A_v K_0(r_{ij}/\lambda_L)$, and the attractive pinning potential is given by $U^{vp}(r_{ip}) = -\alpha_p e^{-(r_{ip}/R_p)^2}$. In these expressions A_v and α_p are tunable parameters, λ_L is the magnetic penetration depth, and $\epsilon_0 = (\phi_0/4\pi\lambda_L)^2$ is an energy per unit length. We consider periodic boundary conditions of (L_x, L_y) sizes in the (x, y) plane. All details about our method for computing the Bessel potential with periodic conditions can be found in [11]. Molecular Dynamics simulation is used for $N_v = 30$ vortices in a rectangular basic cell $(L_x, L_y) = (5, 6\sqrt{3}/2)\lambda_L$. The number of pinning centers is set to $N_p = 30$. We consider the London limit $\kappa = \lambda_L/\xi = 90$, where ξ is the superconducting coherence length [12]. The average vortex distance a_0 is set to $a_0 = \lambda_L$, and $R_p = 0.22 \lambda_L$, $\eta = 1$, $A_v = 2.83 \times 10^{-3} \lambda_L$. We present results for two different pinning strengths corresponding to a maximum pinning force of $F_{max}^{vp} \sim 0.2F_0$ and $F_{max}^{vp} \sim 1.4F_0$, where $F_0 = 2\epsilon_0 A_v/\lambda_L$ is a force defined by the Bessel interaction. In the weak pinning case, the driving force applied along a principal vortex lattice direction x is varied from 0 up to $F^L \sim 3F_0 \sim 100F_c^L$, where F_c^L is the critical Lorentz force along x . In the strong pinning case, the driving force is varied from 0 up to $F^L \sim 3F_0 \sim 20F_c^L$. The choice of the double precision Runge-Kutta algorithm time iteration step δt is dictated by the dominant force, and for example in the high driving phase we take $\delta t = 10^{-3} t_0$, where $t_0 = \eta\lambda_L/F_{max}^L$.

The "experimental" procedure is the following: we start by randomly throwing in the (x, y) plane N_v vortices and N_p gaussian pins, and relaxation with zero

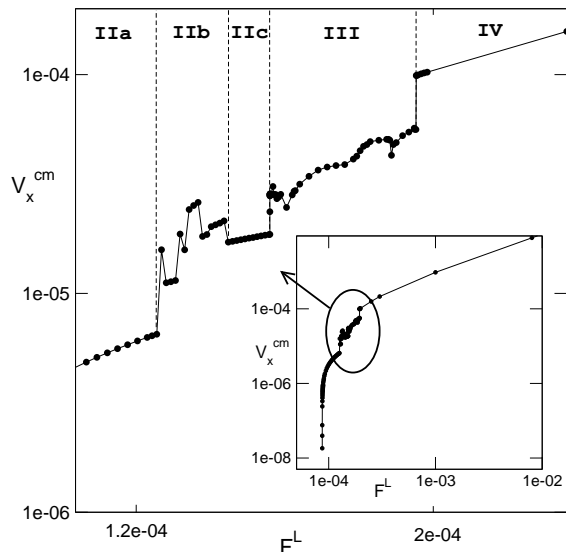


Figure 1: Velocity-force curve obtained in the weak pinning case $F_{max}^{vp} \sim 0.2F_0$. The inset displays the whole curve from depinning regimes up to the high driving phase. An enlargement of the circled region is also displayed and the different observed dynamical regimes are numbered (see text for details).

Lorentz force yields a vortex structure with dislocations. The Lorentz force is then slowly increased up to far in the high driving phase. The inset of Fig. 1 displays the whole velocity-force curve we observe in the weak pinning case $F_{max}^{vp} \sim 0.2F_0$. The velocity shown is the longitudinal velocity of the vortex center of mass V_x^{cm} which is averaged in time for each permanent dynamical regime. Note that this curve is equivalent to the $V - I$ curve obtained in transport experiments on superconductors. The successive regimes we observe in Fig. 1 are the following. Phase I: pinned regime where all vortices have zero velocity. Phase II: plastic channels flowing through pinned regions and where the motion is either periodic or quasiperiodic as seen in [3]. The opening of the first channel (phase IIa) gives rise to a periodic regime where all moving vortices inside the channel replace their respective neighbour within the same time (period). Then, the opening of new channels (phase IIb) leads to quasiperiodic regimes when the different channels don't synchronize their velocity. However the different channels may synchronize their own velocity (*i.e.* rational ratio of their frequency) resulting in a periodic regime for V_x^{cm} . Finally, the last periodic regime observed (phase IIc) corresponds to a single channel mainly aligned with the applied force. Phase III: plastic flow with almost no stationary vortices as seen in [3, 5, 13]. In the following this motion shall be shown to be chaotic. Phase IV: fully elastic flow where the motion occurs through rough static channels. Vortices have the same average velocity and no dislocation appears. Although our numerical results are 2D, we may

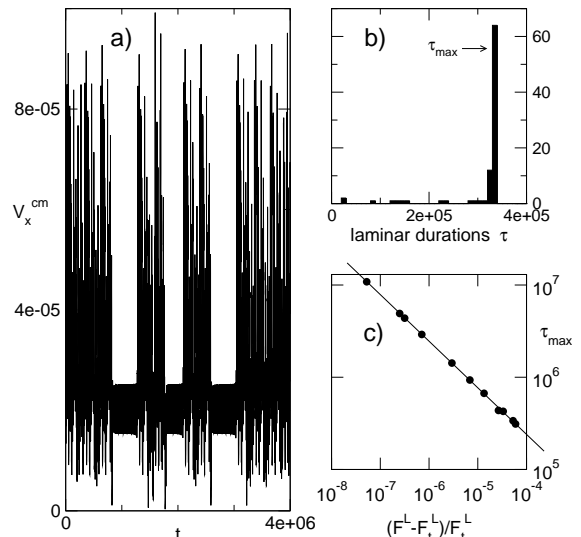


Figure 2: Properties of the transition region from phase IIc to phase III in the weak pinning case $F_{max}^{vp} \sim 0.2F_0$. It clearly displays the type I intermittency route to chaos characteristics. a) part of the time evolution of the longitudinal velocity $V_x^{cm}(t)$ obtained for $F^L = 1.5221 \times 10^{-4}$. One sees laminar (*i.e.* periodic) phases interrupted by chaotic bursts of large velocity fluctuations. b) distribution of the laminar phase durations of $V_x^{cm}(t)$ measured for $F^L = 1.5221 \times 10^{-4}$. In particular, such distribution is characterized by a maximum at an upper bound τ_{max} . c) evolution of τ_{max} when varying the applied force F^L from the intermittency threshold force F_t^L . A clear power law is observed as shown with the line of slope $-1/2$.

call this dynamical regime "moving Bragg glass" as described in the moving glass theory [14].

We shall now focus on the transition from phase IIc to phase III in the weak pinning case $F_{max}^{vp} \sim 0.2F_0$ (Fig. 1). In this very short applied force range, the typical velocity we measure in time is shown in Fig. 2a. It shows time intervals where the motion is periodic (the same as used to exist in phase IIc below the transition). The difference is now that such periodic regime becomes unstable and gives way to a chaotic burst displaying large velocity fluctuations. Then the system goes back to the periodic regime which is still unstable, giving way to another chaotic burst, and so on. The chaotic bursts correspond to apparently disordered trajectories of the moving vortices. However, from time to time, moving vortices are able to synchronize temporarily their motion into the channel (now unstable) of phase IIc giving rise to periodic motion (laminar phases). In the framework of the dissipative chaos theory, such intermittent regimes are known to be one possible way to drive the system from periodicity to chaos. The intermittency "route to chaos" has several characteristics and may be mainly classified in three types (I, II and III) [15, 16]. To determine the type of intermittency we observe in our system, we first measure for a given value of the applied force the distribu-

tion of the laminar (*i.e.* periodic) phase durations. Fig. 2b shows such distribution obtained for $V_x^{cm}(t)$ shown in Fig. 2a. This distribution of laminar phase durations shows a maximum at an upper bound τ_{max} and a decrease for low durations which can be much smaller than τ_{max} . Furthermore, if we now increase very slowly the applied force in order to remain in an intermittent regime, the value of τ_{max} decreases as shown in Fig. 2c. A very nice power law $\tau_{max} \sim (F^L - F_t^L)^{-1/2}$ on almost four decades is measured, where F_t^L is the intermittency threshold, *i.e.* the force above which periodic regimes become unstable. The particular shape of the distribution of the laminar phase durations and the exponent $-1/2$ are characteristics of type I intermittency route to chaos [15, 16]. Note that the type of intermittency may change for different pinning strengths (for stronger pinning parameters $F_{max}^{vp} \sim 1.4F_0$, we observed for example a type II intermittency route to chaos characterized in particular by a different shape of the distribution of the laminar phase durations). Further increasing the applied force will give intermittent regimes with shorter laminar phase durations until they completely disappear therefore giving way only to large chaotic fluctuations. Chaos is then fully developed in phase III.

To examine in details the chaotic phase we shall focus on the strong pinning case $F_{max}^{vp} \sim 1.4F_0$. Let us first examine the successive dynamical regimes. We plot in Fig. 3 the differential resistance curve dV_x^{cm}/dF^L which reproduces the well-known peak [1, 4, 6]. Similarly to the weak pinning regime of Fig. 1, we observe in the strong pinning case of Fig. 3 a depinning threshold followed by periodic and quasiperiodic regimes (phase II). In accordance with Ref. [6], our results also show that the differential resistance peak coincides with the onset of transverse order of the smectic phase [17] since the lattice structure factor (not shown) displays two peaks at $\mathbf{q} = (0, \pm 2\pi/a_0)$ above the differential resistance peak (phase IIIb). In phase IIIb vortices move within channels mainly aligned with the applied force, and transverse jumps of vortices from one channel to another occur (see the non zero transverse velocity V_y^{cm} in Fig. 3). Finally as shown in [6] a dynamical freezing transition occurs when the transverse velocity goes to zero (no more jumps of vortices between the channels) giving rise to the decoupled channels regime (phase IV) named moving transverse glass [14] or smectic phase [17].

We now examine these results in the light of non-linear dynamical systems. In the phase space a dissipative chaotic system evolves in the so-called "strange attractor" because of its fractal dimension. A property of such an attractor is the "sensitive dependence on initial conditions", reflecting the fact that two initial conditions as close as possible on the strange attractor will give rise to two trajectories exponentially diverging in time. The exponents which measure these exponential behaviors are called the Lyapunov exponents. Nega-

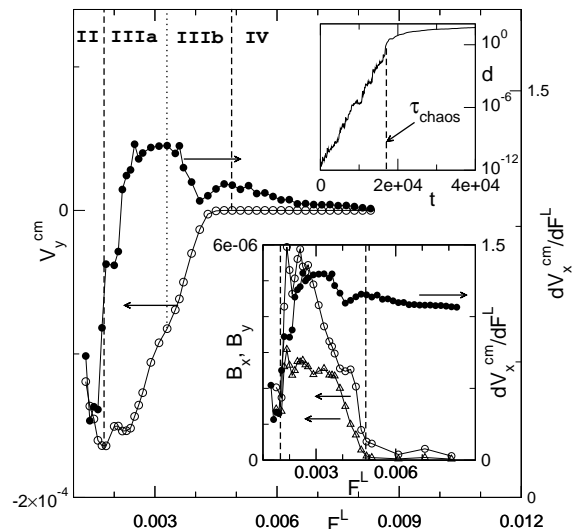


Figure 3: Differential resistance curve (filled circles) and transverse velocity of the center of mass V_y^{cm} (open circles) obtained in the strong pinning case $F_{max}^{vp} \sim 1.4F_0$. The different observed dynamical regimes are numbered (see text for details). The lower right inset displays again the differential resistance curve (filled circles) but also the low frequency longitudinal B_x (open circles) and transverse B_y (triangles) noises. Dotted lines recall the dynamical phases II, III and IV. The upper right inset displays the time evolution of the distance $d(t)$ between two initial neighbouring trajectories in the phase space. Data are shown for $F^L = 0.0029$ in the strong pinning case $F_{max}^{vp} \sim 1.4F_0$. The exponential divergence characteristic of chaos is obvious for $t < \tau_{chaos}$. For time scales larger than τ_{chaos} diffusive motion is observed as already shown in [6].

tive exponents in all directions of the phase space correspond to a fixed point and if one of the exponent is zero the attractor is a limit cycle. A positive exponent is a signature of chaotic dynamics into a strange attractor. To compute the maximal Lyapunov exponent of our system we consider two very close initial conditions and observe how the distance $d(t)$ in the phase space between the two corresponding trajectories evolves in time. Since we integrate N_v first order differential equation of motion (Eq. 1), the phase space is defined by the $2N_v$ vortex coordinates and the distance d is defined by $d^2(t) = \sum_{i=1}^{N_v} \left[\left(X_i(t) - \tilde{X}_i(t) \right)^2 + \left(Y_i(t) - \tilde{Y}_i(t) \right)^2 \right]$ where $X_i(t) = x_i(t) - x_{cm}(t)$, $Y_i(t) = y_i(t) - y_{cm}(t)$, $\tilde{X}_i(t) = \tilde{x}_i(t) - \tilde{x}_{cm}(t)$, $\tilde{Y}_i(t) = \tilde{y}_i(t) - \tilde{y}_{cm}(t)$. In these expressions, (x_i, y_i) and $(\tilde{x}_i, \tilde{y}_i)$ are the vortex i coordinates, and (x_{cm}, y_{cm}) and $(\tilde{x}_{cm}, \tilde{y}_{cm})$ are the respective coordinates of the center of mass. The tilde notation (\tilde{x}, \tilde{y}) refers to the second trajectory generated by the neighbouring initial condition. The upper right inset of Fig. 3 displays an example of the time evolution of d we typically find in phases IIIa and IIIb of Fig. 3. It clearly shows an exponential divergence $d \sim \exp(\lambda t)$ of the two

trajectories for time scales up to $\tau_{chaos} \sim 1.6 \times 10^4 \sim 50t_0$. The slope therefore defines a positive maximal Lyapunov exponent λ characteristic of chaotic dynamics. Note that the fluctuations of $d(t)$ around the slope λ express the fractal nature of the strange attractor associated to the chaotic dynamics. Note also that for time scales larger than τ_{chaos} we find diffusive and superdiffusive motions (not shown) in the transverse and longitudinal directions as already reported in [6]. For a given applied force we compute the power spectrum $S_\nu(f)$ of $V_\nu^{cm}(t)$, *i.e.* $S_\nu(f) = \frac{1}{t_2-t_1} \left| \int_{t_1}^{t_2} dt V_\nu^{cm}(t) \exp(i2\pi ft) \right|^2$ where $\nu = x$ or y , and $t_2 - t_1 \gg \tau_{chaos}$. We define the low frequency noise B_ν by averaging $S_\nu(f)$ over the low frequency range [18]. B_x and B_y are in some way a measure of the degree of chaos in the system since chaotic dynamics generates broad-band noise at low frequencies [16]. Concomitantly with the differential resistance we plot in the lower right inset of Fig. 3 the longitudinal B_x and transverse B_y low frequency noises. The rapid increasing of B_x and B_y confirm the (rapid) setting of chaos in the vortex lattice. When B_x and B_y have raised their maximum value the chaos is fully developed (phase IIIa). In Fig. 3 one can see that this rapid increase of chaos coincides with the beginning of transverse motion destruction since the absolute value of the transverse velocity V_y^{cm} starts to decrease.

We therefore showed evidence for chaos in phase III. As seen in the lower right inset of Fig. 3, the freezing transition coincides with the end of chaos since the low frequency noises B_x and B_y drop to zero. We therefore find that the bottom of the differential resistance peak marks the onset of chaos, while the dynamical freezing transition [6] appears as a transition between chaos and an almost ordered phase (decoupled channels).

In conclusion, we obtained conclusive results about the chaotic dynamics of vortices in the plastic phase. The route to chaos has been identified in details: type I (II) intermittency in the weak (strong) pinning case is found. Chaos characterized by positive Lyapunov exponents and broad band noise is found to coincide with the differential resistance peak. Smectic ordering which appears at the peak is characterized by chaotic dynamics resulting in transverse jumps of vortices between channels. The dynamical freezing transition that occurs above the peak appears as a transition between chaos and the decoupled channel regime.

Therefore our results open new perspectives in the theoretical understanding of the plastic flow phase which is much less developed than the fast moving vortex phases [14, 17] and than the plastic depinning transition [9]. The usual tools of the chaos theory (*e.g.* bifurcation theory, embedding dimensions, Poincaré sections, strange attractors, time series analysis) may help in further theoretical, numerical and experimental investigations of the open issues related to the formation of fractal objects in the complex space phase of driven plastic vortices. Finally, our

results let foresee new possibilities of controlling vortex motion for device applications using the concept of *controlling chaos* developed these last years (see *e.g.* [19]). The goal of such control procedure is to lock the chaotic system into a stable periodic orbit which either used to be unstable in the uncontrolled system (feedback scheme by weakly changing parameters [20]), or which is newly created (non-feedback scheme by weakly forcing the system, see *e.g.* [21]). We therefore suggest that the concept of controlling chaos might be used to design device applications to rectify plastic (chaotic) vortex motion.

We are grateful to the LMPT-CNRS UMR 6083 - Tours (France) for our extensive use of their computers. We acknowledge discussions with T. Giamarchi, P. Le Doussal, A. Mouchet, H. Giacomini and Y. Lansac.

-
- [1] M. J. Higgins, S. Bhattacharya, *Physica C* **257**, 232 (1996); S. Bhattacharya, M. J. Higgins, *Phys. Rev. Lett.* **70**, 2617 (1993).
 - [2] M.W. Rabin *et al.*, *Phys. Rev. B* **57**, R720 (1998); A. M. Troyanovski, J. Aarts, P. H. Kes, *Nature (London)* **399**, 665 (1999); Z.L. Xiao, E.Y. Andrei, M.J. Higgins, *Phys. Rev. Lett.* **83**, 1664 (1999); A. Maeda *et al.*, *Phys. Rev. B* **65**, 54506 (2002); S. Okuma, M. Kamada, *ibid.* **70**, 14509 (2004).
 - [3] N. Gronbech-Jensen, A. R. Bishop, D. Dominguez, *Phys. Rev. Lett.* **76**, 2985 (1996).
 - [4] M. C. Faleski, M. C. Marchetti, A. A. Middleton, *Phys. Rev. B* **54**, 12427 (1996); S. Ryu *et al.*, *Phys. Rev. Lett.* **77**, 5114 (1996); C. J. Olson, C. Reichardt, F. Nori, *ibid.* **81**, 3757 (1998).
 - [5] S. Spencer, H. J. Jensen, *Phys. Rev. B* **55**, 8473 (1997).
 - [6] A. B. Kolton, D. Dominguez, N. Gronbech-Jensen, *Phys. Rev. Lett.* **83**, 3061 (1999).
 - [7] M. Cha, H. Fertig, *Phys. Rev. Lett.* **80**, 3851 (1998); **83**, 2283 (1999); C. Reichardt, K. Moon, R. Scalettar, G. Zimanyi, *ibid.* **83**, 2282 (1998); A. van Otterlo, *ibid.* **84**, 2493 (2000); M. Chandran, R.T. Scalettar, G.T. Zimanyi, *Phys. Rev. B* **67**, 52507 (2003).
 - [8] Y. Paltiel *et al.*, *Nature (London)* **403**, 398 (2000).
 - [9] K. Saunders, J.M. Schwarz, M.C. Marchetti, A.A. Middleton, *Phys. Rev. B* **70**, 24205 (2004), and references therein.
 - [10] J. Levy, M.S. Sherwin, J. Theiler, *Phys. Rev. B* **48**, 7857 (1993); V.I. Marconi, A.B. Kolton, D. Dominguez, N. Gronbech-Jensen, *ibid.* **68**, 104521 (2003).
 - [11] E. Olive, E.H. Brandt, *Phys. Rev. B* **57**, 13861 (1998).
 - [12] ξ appears in the inner cutoff which removes the logarithmic divergence of $K_0(r/\lambda_L)$ at $r \rightarrow 0$ (see Ref. [11]).
 - [13] H. Fangohr, S. J. Cox, P. A. J. de Groot, *Phys. Rev. B* **64**, 064505 (2001).
 - [14] T. Giamarchi, P. Le Doussal, *Phys. Rev. Lett.* **76**, 3408 (1996); *ibid.* **78**, 752 (1997); P. Le Doussal, T. Giamarchi, *Phys. Rev. B* **57**, 11356 (1998).
 - [15] Y. Pomeau, P. Manneville, *Commun. Math. Phys.* **74**, 189 (1980).
 - [16] P. Bergé, Y. Pomeau, and C. Vidal, *Order within Chaos* (Wiley-Interscience, New York, 1986).

- [17] L. Balents, M. C. Marchetti, L. Radzihovsky, Phys. Rev. Lett. **78**, 751 (1997); Phys. Rev. B **57**, 7705 (1998).
- [18] In our system we differentiate the low and very low frequency ranges: the very low frequency range $f < 1/\tau_{chaos}$ characterizes the diffusive motion, whereas the low frequency range $1/\tau_{chaos} < f \ll \lambda$ corresponds to the chaotic behavior, where λ is the Lyapunov exponent.
- [19] H.D.I. Abarbanel, R. Brown, J.J. Sidorowich, L. Sh. Tsimring, Rev. Mod. Phys. **65**, 1331 (1993).
- [20] E. Ott, C. Grebogi, J.A. Yorke, Phys. Rev. Lett. **64**, 1196 (1990); W.L. Ditto, S.N. Rausero, M.L. Spano, *ibid.* **65**, 3211 (1990).
- [21] Y. Braiman, I. Goldhirsch, Phys. Rev. Lett. **66**, 2545 (1991).